Electric Power Systems Research 214 (2023) 108942

Contents lists available at ScienceDirect

Electric Power Systems Research

journal homepage: www.elsevier.com/locate/epsr

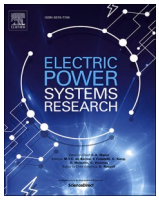

Small-signal stability analysis of the asymmetrical DC operation in HVDC networks

Jesús Serrano-Sillero, M. Ángeles Moreno *

Universidad Carlos III de Madrid, Avda. Universidad 30, Leganés, 28911, Spain

ARTICLE INFO

Keywords:
Asymmetrical DC operation
MMC-VSC converters
Grounding system
Small-signal stability
Observability
Controllability

ABSTRACT

The increase in High Voltage Direct Current (HVDC) projects favors their future interconnection to form regional networks, but this interconnection can be hindered by the lack of standardization in station's configuration and converter's differing grounding schemes. Whilst other studies have studied the effect of Direct Current (DC) asymmetrical operation, they are limited in their scope. This paper proposes a more realistic perspective, considering stations with different topologies, permanent DC asymmetries and the influence of the grounding systems. This more complex point of departure requires the re-examination of the modeling methods, from time-domain to frequency-domain. This paper proposes a small-signal stability model of the system, which is validated with the electromagnetic transient (EMT) dynamic simulations using PowerFactory. This model provides guidelines for designing the grounding impedance and allows the proper design of a specific controller to dampen the asymmetrical DC operation mode.

1. Introduction

The number of commissioned and planned HVDC projects based on Voltage Source Converter (VSC) technology in Modular Multilevel Converter (MMC) topology has increased worldwide in recent years [1,2] and HVDC links are likely to progressively interconnect forming regional multiterminal DC (MTDC) networks [2–4]. Because of the lack of standardization, different station configurations and grounding schemes could coexist in such networks. Therefore, unless DC-DC converters that also include galvanic isolation are used for the interconnections, the protection system and the operation of the entire HVDC network during a DC pole imbalance can be affected as a result of the grounding system interconnection. However, DC-DC converters with galvanic isolation may not always be the best option [4–6].

The repercussions of the grounding impedance in the insulation of the equipment and the fault protection methods have been widely discussed in the literature [5–9]. Although some works have dealt with the relationship between the grounding impedance and the asymmetrical DC operation, they have not examined the implications of the grounding system in networks where different HVDC station topologies exist or in case of permanent DC asymmetries. The influence of the grounding resistance on the resulting DC asymmetry after a contingency was addressed in [10] from a steady-state perspective. Reference [11] proved that each pole of a symmetrical monopolar HVDC station can be controlled independently using its AC grounding system, but the study was addressed in a DC network with only an HVDC station. The DC voltage pole imbalance and different methods for rebalancing were analyzed in [12,13], but the focus was put on the transient DC asymmetry after a pole to ground fault in a network with a single HVDC station topology. Similarly, [7–9, 12,14] also described controllers aimed to avoid the asymmetrical DC operation but, again, they were only valid for the transient DC asymmetry after clearing a pole-to-ground fault and might cause undesired voltage levels in case of a permanent DC asymmetry.

This paper analyzes how the asymmetrical DC operation affects the stability of a system of the mentioned characteristics. Most research papers in literature assess stability from a symmetrical DC operation perspective. For example, the control interactions and their design were analyzed in [15,16]; the effect of a new connection of an HVDC station on DC voltage stability was studied in [17]; [18,19] examined the influence of the DC power flow direction on stability; power and DC voltage oscillations were investigated in [20,21]. Even the stability of systems with line-commutated converters (LCCs) and VSCs has been evaluated [21,22]. Nonetheless, all the mentioned works neglected relevant aspects to analyze asymmetrical DC operation, such as representing the quantities of the positive and negative poles separately or including the grounding system in the analysis.

* Corresponding author.
E-mail address: mangeles.moreno@uc3m.es (M.Á. Moreno).

https://doi.org/10.1016/j.epsr.2022.108942
Received 21 July 2022; Received in revised form 13 October 2022; Accepted 30 October 2022
Available online 10 November 2022

Nomenclature

Superscripts

b	Bipolar converter/station.
m	Monopolar converter/station.
*	Reference value.
+/-	Positive/negative pole.

Subscripts

$d,q,0$	Direct/quadrature/zero-sequence components.
o	Initial operating point.

Variables

i_c^{b+}, i_c^{b-}	Positive/negative pole current on the ac side of the bipolar converter.
i_c^m	Current on the ac side of the monopolar converter.
i_{dc}^{b+}, i_{dc}^{b-}	Positive/negative pole current on the dc side of the bipolar converter.
i_{dc}^{m+}, i_{dc}^{m-}	Positive/negative pole current on the dc side of the monopolar converter.
i_e	Earth current.
i_g^m, i_g^b	Current injected by the external ac grid on the ac side of the monopolar/bipolar station.
$i_{c,d}^m, i_{c,q}^m, i_{c,0}^m$	Direct/quadrature/zero-sequence current components on the ac side of the monopolar converter.
$i_{c,d}^{*m}, i_{c,q}^{*m}$	References for the direct/quadrature current components on the ac side of the monopolar converter.
i_{line}^+, i_{line}^-	Positive/negative pole current on the dc line.
$i_{trf}^{b+}, i_{trf}^{b-}$	Current on the transformer of the positive/negative pole of the bipolar converter.
$p_{ctrl}^{*m}, q_{ctrl}^{*m}$	References for the active/reactive power of the controllers at monopolar converter.
v_c^{b+}, v_c^{b-}	Internal ac voltage of the positive/negative pole of the bipolar converter.
v_c^m	Internal ac voltage of the monopolar converter.
$v_{c,d}^m, v_{c,q}^m, v_{c,0}^m$	Direct/quadrature/zero-sequence components of the internal ac voltage of the monopolar converter.
v_{com}^b	Voltage at the common point of the bipolar converter.
$v_{ctrl}^{b+}, v_{ctrl}^{b-}$	AC voltage at the point controlled by the positive/negative pole of the bipolar converter.
v_{ctrl}^m	AC voltage at the point controlled by the monopolar converter.
$v_{ctrl.d}^m, v_{ctrl.q}^m$	Direct/quadrature components of the ac voltage at the point controlled by the monopolar converter.
v_{ctrl}^{*m}	AC voltage reference for the monopolar converter controller.
v_{dc}^{b+}, v_{dc}^{b-}	Positive/negative pole voltage on the dc side of the bipolar converter.
v_{dc}^{m+}, v_{dc}^{m-}	Positive/negative pole voltage on the dc side of the monopolar converter.
v_{dc}^{*m}	DC voltage reference for the monopolar converter controller.
v_g^m, v_g^b	AC grid Thevenin voltage on the ac side of the monopolar/bipolar station.
v_n	Difference between pole DC voltages of the monopolar converter.
s_x	Insertion indexes of the submodules of each arm.
θ_{pll}	Reference frame angle θ generated by the phase-locked loop of the converter.

Parameters

r_e	Grounding resistance for the zig-zag transformer.
l_e	Equivalent inductance of the zig-zag transformer.
r_g, l_g	Thévenin resistance and inductance of the external AC grid.
r_{line}, l_{line}	Series resistance and inductance of the π-model of the dc line.
r_{trf}, l_{trf}	Series resistance and inductance of the converter transformer.
r_{arm}, l_{arm}	Resistance and inductance of the converter arms.
l_{cc}	AC equivalent inductance from the converter to the controlled point.
c_c	Equivalent capacitance of converter submodules.
c_f	Fictitious capacitance located to make voltage a state variable.
c_{line}	Half capacitance of the π-model of the dc line.
ω_g	Grid frequency.
ω_b	Base frequency.
kp_{vdc}, ki_{vdc}	Proportional and integral gains of the DC voltage controller.
kp_{vac}, ki_{vac}	Proportional and integral gains of the AC voltage controller.
kp_p, ki_p	Proportional and integral gains of the active power controller.
kp_q, ki_q	Proportional and integral gains of the reactive power controller.
kp_i, ki_i	Proportional and integral gains of the inner controller.
k_{p0}, k_{do}	Upper/lower path gains of the zero-sequence controller.

In a previous work [23], the authors analyzed a system with both bipolar and symmetrical monopolar HVDC stations connected without galvanic isolation. The effect of the grounding impedance of symmetrical monopolar stations on such a heterogeneous HVDC grid was studied for the first time, demonstrating that the control, the operation point, and the grounding impedance affect stability. Thus, the asymmetrical DC operation should be a factor to consider in the stability analysis, but further research is needed to support conclusions in different circumstances, and the analysis through time-consuming time-domain simulations is not feasible for that purpose, especially in the case of large HVDC systems.

Accordingly, in this paper, a new small-signal model of the system is developed. Furthermore, the small-signal analysis allows the identification of which system parameters are involved in the dynamics related to the asymmetrical DC operation and to define its appropriate values, both for controllers and equipment.

The main contributions of this paper are summarized as follows: (a) the development of a small-signal stability model that is feasible for asymmetrical DC operation studies and grounding systems design; (b) the validation of the small-signal model with electromagnetic transients (EMT) dynamic simulation in PowerFactory; (c) the analysis of the main aspects to be considered for the system operation and design of the grounding impedance from a stability point of view; and (d) the design of a controller that enhances system stability during asymmetrical DC operation.

The paper is organized as follows: Section 2 describes the system used for the study and its small-signal model; Section 3 presents the validation of the small-signal model with EMT dynamic simulation; Section 4 explains the main results derived from the small-signal analysis; Section 5 introduces a controller to enhance the system stability and proves its performance; and finally, the conclusions are gathered in Section 6.

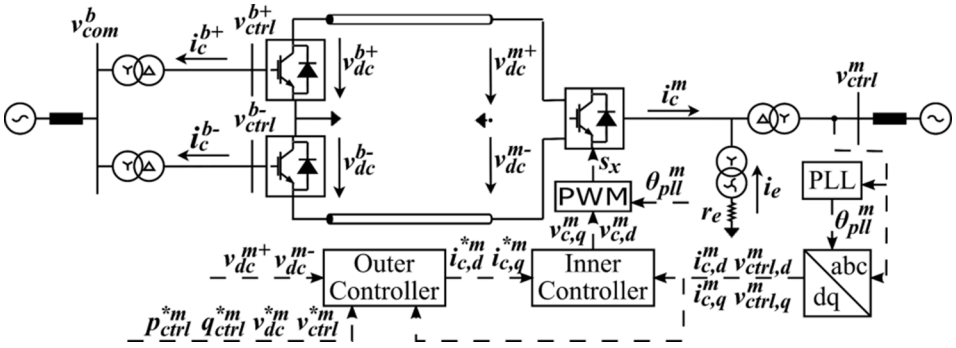

Fig. 1. Connection of a symmetrical monopolar HVDC station with a bipolar one.

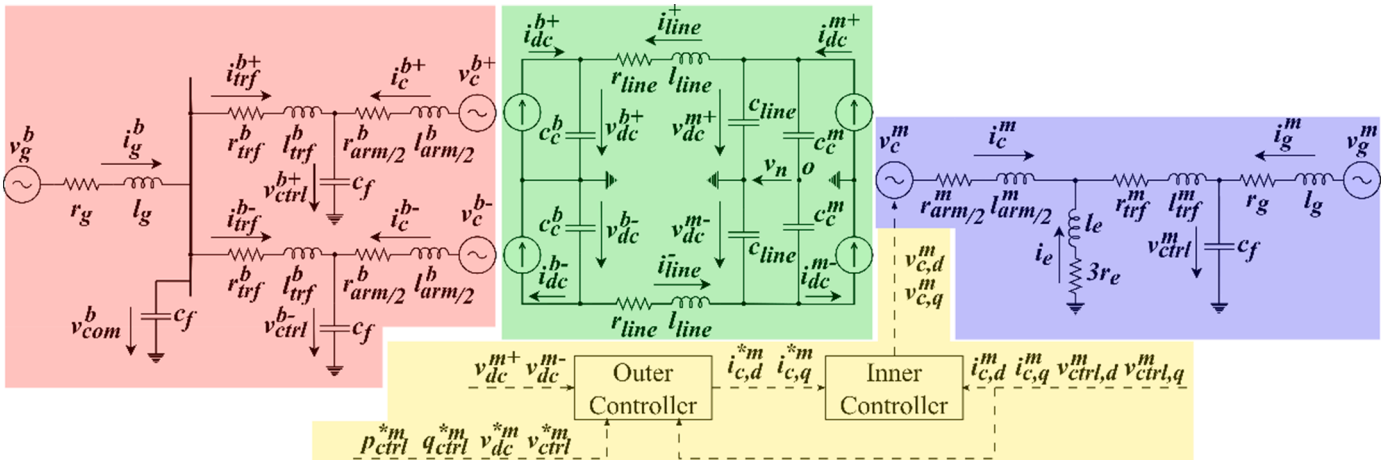

Fig. 2. Per unit equivalent system for the AC side of the bipolar (red) and monopolar (blue) station, the DC side (green) and the control system (yellow).

2. System modeling

To address the analysis of DC asymmetrical operation in a MTDC system where symmetrical monopolar and bipolar topologies coexist without a galvanic isolation between them, a simple model has been considered in PowerFactory. This model consists of a DC link connecting a bipolar station with a symmetrical monopolar one, as shown in Fig. 1. The symmetrical monopolar HVDC station uses a zig-zag transformer as a grounding system, whereas the bipolar HVDC station is solidly earthed. For the MMC-VSCs, the Average Value Model (AVM) is adopted [24,25]. Therefore, the valves are not explicitly modeled, and the AC side is represented through a controlled voltage source on each arm. The capacitor voltages of all submodules are assumed to be equal, thus, no circulating currents flow between the phase legs. The DC side is modeled as a current source with the equivalent capacitance of the submodules in parallel.

Fig. 1 also represents the general control scheme for the symmetrical monopolar HVDC station. An analogous controller applies for each converter of the bipolar station. These controllers are based on those described in [24] and their gains are gathered in Table 2 in the Appendix.

2.1. State-space representation of the system

The system shown in Fig. 1 can be modeled as a compound of three equivalent circuits, as depicted in Fig. 2.

The equivalent circuits in Fig. 2 show positive references for voltages and currents. The values of the passive elements are gathered in the Appendix.

The electrical equations are presented in a synchronous reference frame where the direct axis is aligned with the voltages v^m_{ctrl} and v^{b+}_{ctrl}, respectively. Considering that the bipolar station works symmetrically, the voltage v^{b-}_{ctrl} will be aligned with v^{b+}_{ctrl} and thus also with the direct axis of the synchronous reference frame.

Converters are represented as voltage sources at their AC side (v^m_c, v^{b+}_c and v^{b-}_c) in series with the equivalent impedance of a leg ($\frac{r_{arm}}{2}$ and $\frac{l_{arm}}{2}$). Each converter is connected to its respective AC grid through a transformer represented by its equivalent series impedance (r_{trf} and l_{trf}). The zig-zag transformer of the symmetrical monopolar HVDC station is modeled as an open circuit for the positive and negative sequences, but as an equivalent inductance per phase (l_e) and an equivalent resistance from the star point to ground (r_e) for the zero-sequence. The earth current circulating per each phase is represented by i_e. The external AC grids are modeled by Thévenin equivalent circuits. Furthermore, several capacitors (c_f) of small capacitance are located at some busbars of the AC systems for convenience, to make the voltage at that point a state variable.

Regarding the equivalent circuit of the DC system, the current sources at both ends represent the current injection from HVDC stations. The DC current injection from the symmetrical monopolar HVDC station is modeled as two current sources coupled by the expression $i^{m+}_{dc} - i^{m-}_{dc} = 3i_e$. Therefore, when there is no earth current, both sources can be simplified into a single current source injecting a current i^m_{dc}. The equivalent capacitor of the monopolar HVDC station (c^m_{eq}) is divided into two capacitors located between each DC pole and the middle point O, that is, $c^m_c = 2c^m_{eq}$. For the DC line, a nominal π-model is used. At the terminals of the bipolar HVDC station, the corresponding half capacitance of the π-model of the line (c_{line}) is grouped with the equivalent capacitor of each converter of the bipolar HVDC station (c^b_{eq}), so that

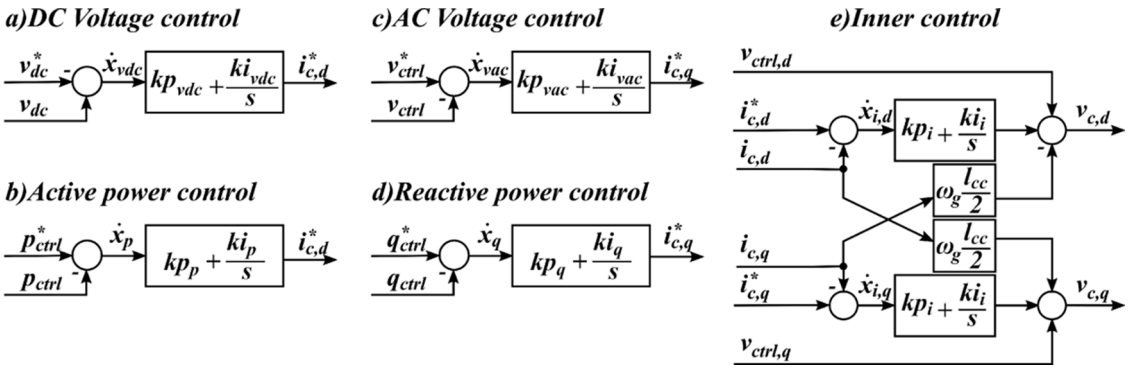

Fig. 3. Outer Control Loops (a-d) and inner control loop (e).

$c_c^b = c_{eq}^b + c_{line}$.

Finally, the coupling between the two AC areas and the DC link is the result of applying the active power balance equation to each converter:

$$v_{c,d}^m \cdot i_{c,d}^m + v_{c,q}^m \cdot i_{c,q}^m + 2 \cdot v_{c,0}^m \cdot i_{c,0}^m = \frac{1}{2}\left(v_{dc}^{m+} \cdot i_{dc}^{m+} + v_{dc}^{m-} \cdot i_{dc}^{m-}\right) \tag{1}$$

$$v_{c,d}^{b\pm} \cdot i_{c,d}^{b\pm} + v_{c,q}^{b\pm} \cdot i_{c,q}^{b\pm} = \frac{1}{2}\left(v_{dc}^{b\pm} \cdot i_{dc}^{b\pm}\right) \tag{2}$$

The inner voltage dynamics of each converter are governed by its control system. Fig. 2 shows the part of the controller that is considered for the development of the linearized model. The same control diagram applies to each converter of the bipolar HVDC station.

The Phase-Locked Loop (PLL) in Fig. 1 is not considered in Fig. 2 since the dynamics of the PLL hardly affect the DC asymmetrical operation.

The outer controller of each converter consists of two independent control loops that generate the active current reference ($i_{c,d}^*$) and the reactive current reference ($i_{c,q}^*$). In this paper, the symmetrical monopolar HVDC station controls the DC voltage and the AC voltage whereas the bipolar HVDC station controls the active and reactive power flow at its AC side. Fig. 3 (a-d) shows the block diagram of the outer control loops.

The inner controller depicted in Fig. 3(e) computes the components of the converter inner voltage in the synchronous reference frame ($v_{c,d}$ and $v_{c,q}$).

The set of equations that describe the complete control of each converter, together with the electrical equations from Fig. 2, constitute the state-space representation of the system. The values for the control parameters are gathered in the Appendix.

2.2. Small-signal modeling

The state-space model representation comprises a nonlinear system that can be linearized around an operating point to obtain a small-signal model in the form of (3).

$$\Delta\dot{\mathbf{x}} = \mathbf{A}\cdot\Delta\mathbf{x} + \mathbf{B}\cdot\Delta\mathbf{u} \tag{3}$$

The state variables vector $\Delta\mathbf{x}$ consists of six sub-vectors that contain the states of the six subsystems that make up the complete system (AC side of the monopolar HVDC station, AC side of the bipolar HVDC station, DC electrical system, and control system of each converter):

$$\Delta\mathbf{x} = \left[\Delta\mathbf{x}_{\mathbf{ac}}^{\mathbf{m}}\ \Delta\mathbf{x}_{\mathbf{ac}}^{\mathbf{b}}\ \Delta\mathbf{x}_{\mathbf{dc}}\ \Delta\mathbf{x}_{\mathbf{ctrl}}^{\mathbf{m}}\ \Delta\mathbf{x}_{\mathbf{ctrl}}^{\mathbf{b}+}\ \Delta\mathbf{x}_{\mathbf{ctrl}}^{\mathbf{b}-}\right]^T \tag{4}$$

These state vectors are described in (5)-(10):

$$\Delta\mathbf{x}_{\mathbf{ac}}^{\mathbf{m}} = \left[\Delta i_{c,d}^m\ \Delta i_{c,q}^m\ \Delta i_{g,d}^m\ \Delta i_{g,q}^m\ \Delta v_{ctrl,d}^m\ \Delta v_{ctrl,q}^m\right] \tag{5}$$

$$\Delta\mathbf{x}_{\mathbf{ac}}^{\mathbf{b}} = \left[\Delta i_{c,d}^{b+}\ \Delta i_{c,q}^{b+}\ \Delta i_{trf,d}^{b+}\ \Delta i_{trf,q}^{b+}\ \Delta v_{ctrl,d}^{b+}\ \Delta v_{ctrl,q}^{b-}\ \Delta i_{c,d}^{b-}\ \Delta i_{c,q}^{b-}\cdots \cdots \Delta i_{trf,d}^{b-}\ \Delta i_{trf,q}^{b-}\ \Delta v_{ctrl,d}^{b-}\ \Delta v_{ctrl,q}^{b-}\ \Delta i_{g,d}^{b}\ \Delta i_{g,q}^{b}\ \Delta v_{com,d}^{b}\ \Delta v_{com,q}^{b}\right] \tag{6}$$

$$\Delta\mathbf{x}_{\mathbf{dc}} = \left[\Delta v_{dc}^{m+}\ \Delta v_{dc}^{m-}\ \Delta v_{dc}^{b+}\ \Delta v_{dc}^{b-}\ \Delta i_{line}^{+}\ \Delta i_{line}^{-}\ \Delta i_e\right] \tag{7}$$

$$\Delta\mathbf{x}_{\mathbf{ctrl}}^{\mathbf{m}} = \left[\Delta x_{i,d}^m\ \Delta x_{i,q}^m\ \Delta x_{vdc}^m\ \Delta x_{vac}^m\right] \tag{8}$$

$$\Delta\mathbf{x}_{\mathbf{ctrl}}^{\mathbf{b}+} = \left[\Delta x_{i,q}^{b+}\ \Delta x_{i,q}^{b+}\ \Delta x_p^{b+}\ \Delta x_q^{b+}\right] \tag{9}$$

$$\Delta\mathbf{x}_{\mathbf{ctrl}}^{\mathbf{b}-} = \left[\Delta x_{i,d}^{b-}\ \Delta x_{i,q}^{b-}\ \Delta x_p^{b-}\ \Delta x_q^{b-}\right] \tag{10}$$

In summary, the small-signal model of the system includes 41 state variables.

Regarding the states Δx_{vac}^m, Δx_q^{b+}, Δx_q^{b-}, Δx_p^{b+}, Δx_p^{b-}, Δv_{dc}^{m+}, Δv_{dc}^{m-}, Δv_{dc}^{b+} and Δv_{dc}^{b-}, the linearization is done by taking into account the equivalent circuits in Fig. 2 and the block diagrams in Fig. 3. The bipolar HVDC station is assumed to operate symmetrically in the initial operating point and therefore no zero-sequence current/voltage is considered. Subscript *o* indicates the value of a variable in the initial operating point. These considerations yield the next expressions:

$$\Delta\dot{x}_{vac}^m \approx -\Delta v_{ctrl,d}^m + \Delta v_{ctrl}^{*m} \tag{11}$$

$$\Delta\dot{x}_p^{b\pm} \approx -v_{ctrl,do}^{b\pm}\cdot\Delta i_{c,d}^{b\pm} - i_{c,do}^{b\pm}\cdot\Delta v_{ctrl,d}^{b\pm} - i_{c,qo}^{b\pm}\cdot\Delta v_{ctrl,q}^{b\pm} + \Delta p_{ctrl}^{*b\pm} \tag{12}$$

$$\Delta\dot{x}_q^{b\pm} \approx -i_{c,do}^{b\pm}\cdot\Delta v_{ctrl,q}^{b\pm} + v_{ctrl,do}^{b\pm}\cdot\Delta i_{c,q}^{b\pm} + i_{c,qo}^{b\pm}\cdot\Delta v_{ctrl,d}^{b\pm} + \Delta q_{ctrl}^{*b\pm} \tag{13}$$

$$\Delta\dot{v}_{dc}^{m+} = \left[\Delta i_{dc}^{m+}\left(1 - \frac{c_c^m}{2\left(c_c^m + c_{line}\right)}\right) - \Delta i_{line}^{+}\left(1 - \frac{c_c^m}{2\left(c_c^m + c_{line}\right)}\right) - \Delta i_{dc}^{m-}\frac{c_c^m}{2\left(c_c^m + c_{line}\right)} + \Delta i_{line}^{-}\frac{c_c^m}{2\left(c_c^m + c_{line}\right)}\right]\frac{\omega_b}{c_{line}} \tag{14}$$

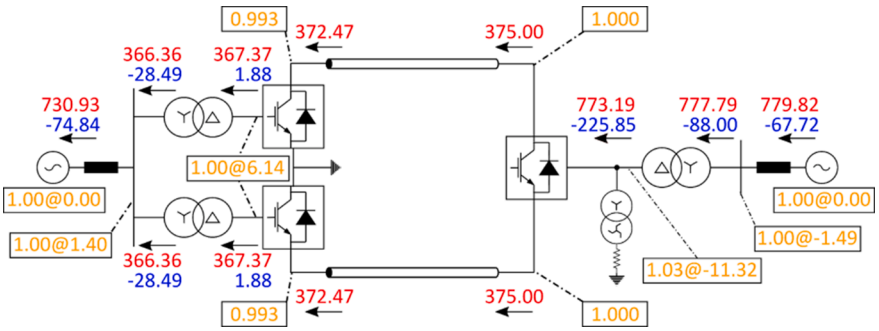

Fig. 4. Initial conditions of the system for the base case.

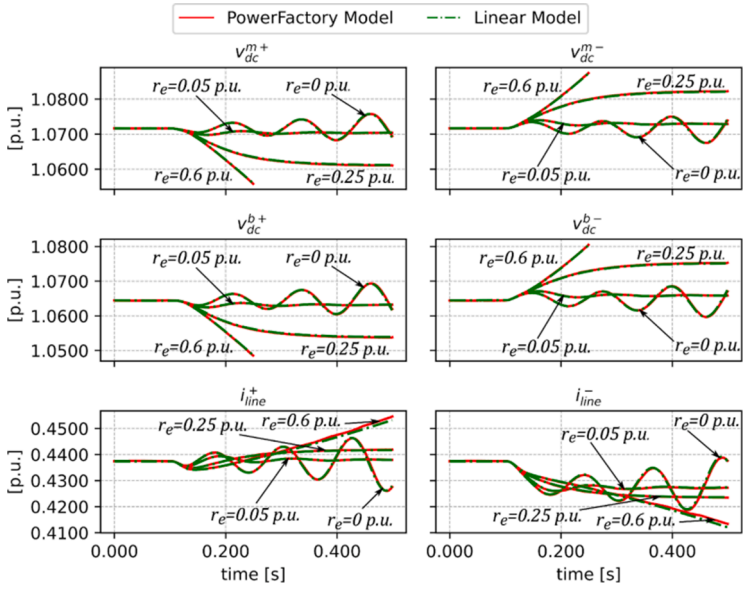

Fig. 5. DC quantities response to a DC asymmetry for several grounding resistances.

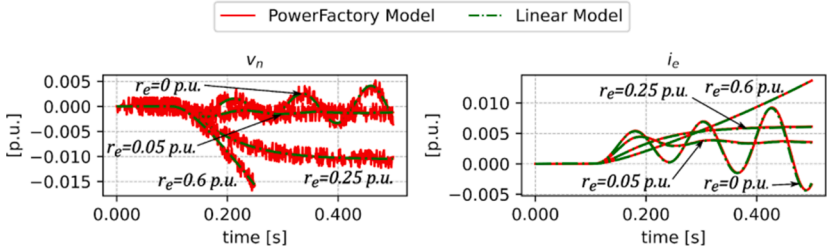

Fig. 6. Zero-sequence voltage and earth current response to a DC asymmetry for several grounding resistances.

$$\Delta\dot{v}_{dc}^{m-} = \left[\Delta i_{dc}^{m-}\left(1-\frac{c_c^m}{2\left(c_c^m+c_{line}\right)}\right)-\Delta i_{line}^{-}\left(1-\frac{c_c^m}{2\left(c_c^m+c_{line}\right)}\right)-\Delta i_{dc}^{m+}\frac{c_c^m}{2\left(c_c^m+c_{line}\right)}+\Delta i_{line}^{+}\frac{c_c^m}{2\left(c_c^m+c_{line}\right)}\right]\frac{\omega_b}{c_{line}} \tag{15}$$

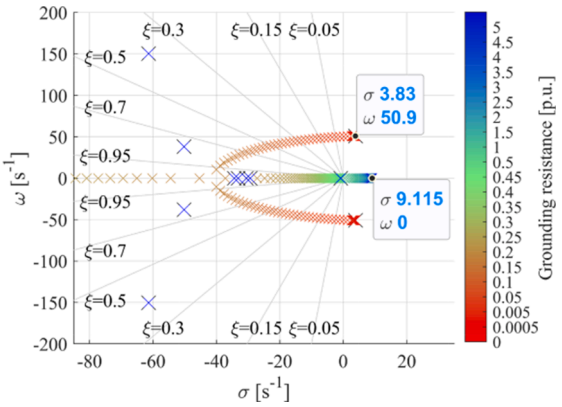

Fig. 7. Root locus of the system for a grounding resistance sweep.

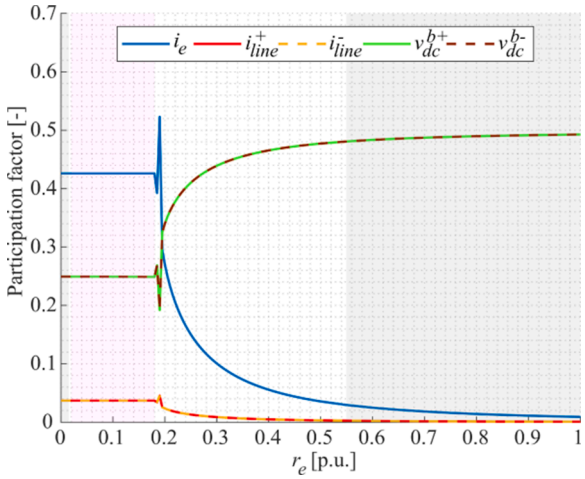

Fig. 8. Participation factor for a range of grounding resistance. The gray, red and white areas represent unstable, underdamped, and overdamped mode, respectively.

$$\Delta v_{dc}^{b\pm} = \left(\Delta i_{dc}^{b\pm} + \Delta i_{line}^{\pm}\right)\frac{\omega_b}{c_c^b}, \tag{16}$$

where the linear expressions that describe the DC currents Δi_{dc}^{m+} and Δi_{dc}^{m-} are presented in (17) and the linear expression for Δi_{dc}^{b+} and Δi_{dc}^{b-} is obtained in (18).

$$\Delta i_{dc}^{m\pm} \approx 2\frac{\left(v_{c,do}^{m}\cdot i_{c,do}^{m} + v_{c,qo}^{m}\cdot i_{c,qo}^{m}\right)}{\left(v_{dc,o}^{m+} + v_{dc,o}^{m-}\right)^2}\left(\Delta v_{dc}^{m+} + \Delta v_{dc}^{m-}\right) - 2\frac{v_{c,do}^{m}\cdot\Delta i_{c,d}^{m} + i_{c,do}^{m}\cdot\Delta v_{c,d}^{m} + v_{c,qo}^{m}\cdot\Delta i_{c,q}^{m} + i_{c,qo}^{m}\cdot\Delta v_{c,q}^{m}}{\left(v_{dc,o}^{m+} + v_{dc,o}^{m-}\right)} \pm \frac{3}{2}\Delta i_e \tag{17}$$

$$\Delta i_{dc}^{b\pm} \approx 2\frac{\left(v_{c,do}^{b\pm}\cdot i_{c,do}^{b\pm} + v_{c,qo}^{b\pm}\cdot i_{c,qo}^{b\pm}\right)}{\left(v_{dc,o}^{b\pm}\right)^2}\Delta v_{dc}^{b\pm} - 2\frac{v_{c,do}^{b\pm}\cdot\Delta i_{c,d}^{b\pm} + i_{c,do}^{b\pm}\cdot\Delta v_{c,d}^{b\pm} + v_{c,qo}^{b\pm}\cdot\Delta i_{c,q}^{b\pm} + i_{c,qo}^{b\pm}\cdot\Delta v_{c,q}^{b\pm}}{v_{dc,o}^{b\pm}} \tag{18}$$

The expressions that define the remaining states of the vector $\Delta\mathbf{x}$ are first-order linear equations that can be drawn directly from Fig. 2 and Fig. 3.

Fig. 4 shows the power flow results for the initial operating point. Red values represent the active power flow in MW and blue values the reactive power flow in Mvar. The black arrows indicate the positive direction of the power flow. Finally, the voltage magnitude, in p.u., and phase angle, in degrees, are represented inside a box.

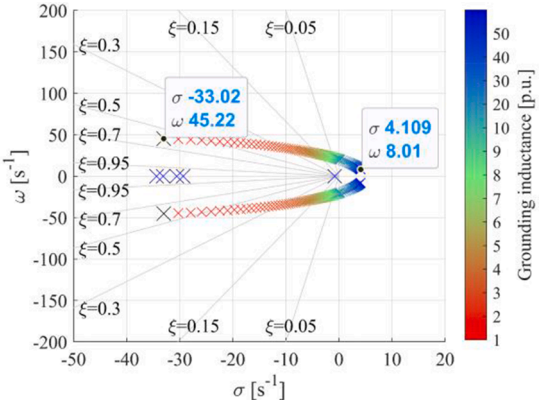

Fig. 10. Root locus of the system for a grounding inductance sweep.

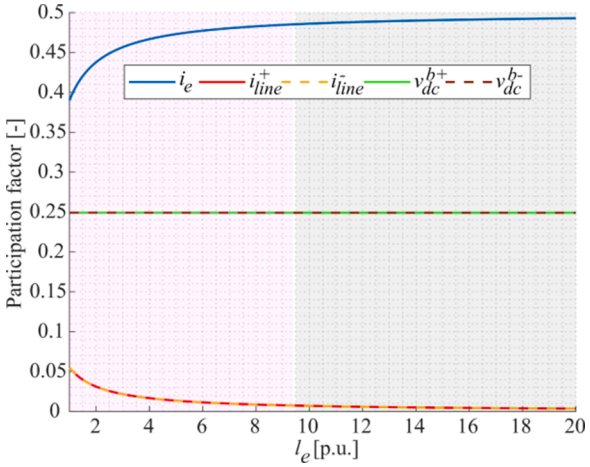

Fig. 11. Participation factors for a grounding inductance range. The gray and red areas represent unstable and overdamped mode, respectively.

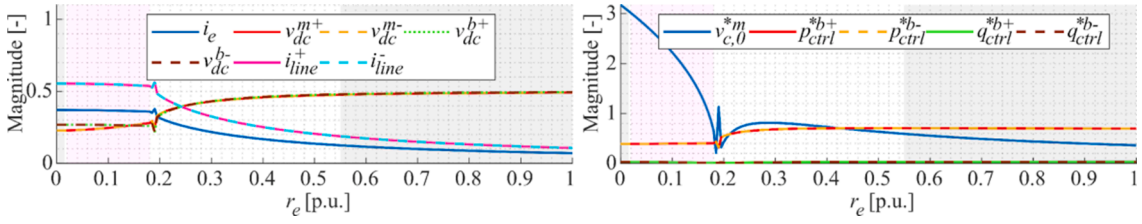

Fig. 9. Mode observability (left) and controllability (right) as a function of grounding resistance. The gray, red and white areas represent unstable, underdamped, and overdamped mode, respectively.

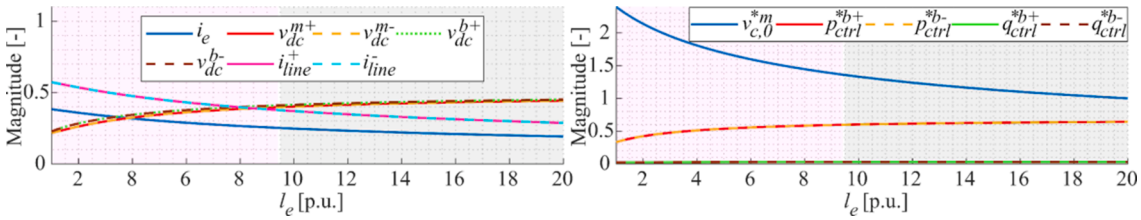

Fig. 12. Mode observability (left) and controllability (right) as a function of the grounding system inductance. The gray and red areas represent unstable and underdamped mode, respectively.

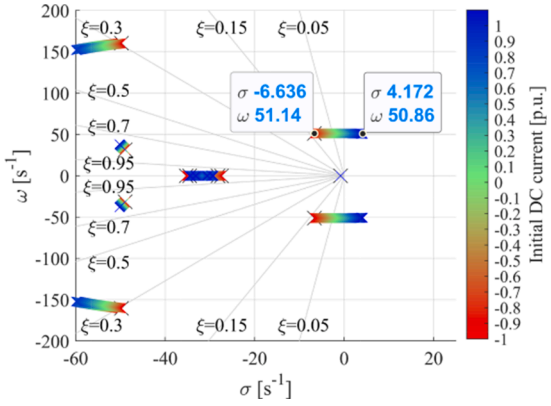

Fig. 13. Root locus of the system as a function of the initial DC current.

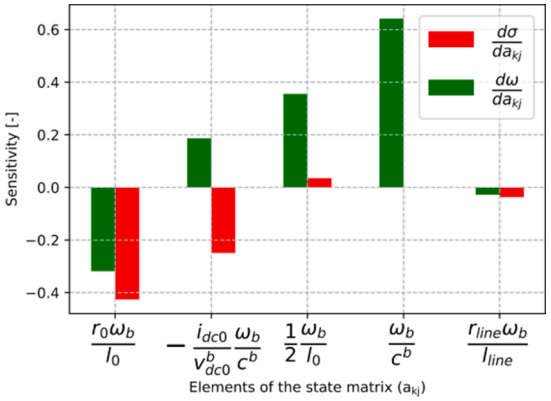

Fig. 14. Sensitivity of the real and imaginary part of the mode.

The operating point shown in Fig. 4 represents a scenario of high active power transfer from the monopolar to the bipolar HVDC station. This scenario is convenient for the analysis because, as it will be explained later, it is under these circumstances that stability is most compromised from the perspective of the asymmetrical DC operation. However, other operating conditions will also be discussed in Section 4.

3. Validation of the small-signal model

To validate the linear model, this section gathers some simulations comparing its response with the response of an EMT simulation in PowerFactory facing an asymmetrical disturbance at the DC side. This disturbance consists of a small step (0.01 p.u.) in the active power reference of the negative pole converter of the bipolar station.

Fig. 5 and Fig. 6 show the comparison of the time-domain responses for several grounding resistance values. The consistency in the time-domain responses of both models allows to validate the new small-signal model.

Different dynamic behaviors can be identified: an unstable and oscillatory for a zero-resistance value, an underdamped response for 0.05 p.u. resistance value, an overdamped response for 0.25 p.u. resistance value and an unstable non-oscillatory response for 0.6 p.u. resistance value (this response is not shown completely to represent the curves on a proper scale). Note that positive and negative DC quantities present an opposite response to one another.

4. Small-signal stability analysis

In this section, the small-signal stability of the system is assessed from different perspectives that cover the following aspects: (a) influence of the grounding impedance; (b) influence of the DC current, and (c) sensitivity to the system parameters.

4.1. Influence of the grounding system resistance

The grounding resistance plays a key role in the asymmetrical DC operation since it determines the behavior of the earth current (i_e) and the zero-sequence voltage (v_n).

The impact of its value on the small-signal stability is analyzed through the root locus of the system in Fig. 7 under the initial conditions described in Fig. 4.

Fig. 7 shows that there is a single mode affected by the grounding resistance in the vicinity of the imaginary axis. This mode is critically damped for a resistance value of 0.19 p.u. and can be underdamped or even non-stable and oscillatory for lower resistance values, as well as overdamped or non-stable aperiodic for larger values.

The normalized participation of the states in the mode as a function of the resistance is depicted in Fig. 8. Only states with participation greater than 0.01 are shown.

As shown in Fig. 8, the main variables participating in the mode are the earth current, the DC current, and the DC voltages at the bipolar station terminals. Around the resistance value matching the critically damped mode, the participation factors change significantly due to the division of the mode into two aperiodic ones [26], representing an interaction between the earth current and the DC currents with the DC voltages.

The dynamic pattern of the mode can be observed in the DC voltages, DC currents, and earth current according to Fig. 9, so it does not spread to the rest of the AC system. Notice that in the overdamped region, as the resistance rises, the observability is hindered for the currents, while it is enhanced for the voltages.

According to Fig. 9, the mode can be controlled by the zero-sequence reference voltage of the monopolar HVDC station and the active power references of the bipolar HVDC station. In particular, the zero-sequence voltage shows high controllability for low grounding resistances where the mode is oscillatory.

It is worth noting that the present controllers have no influence on this specific mode since their states do not participate in it nor is the mode observable in the measurements that the controllers use as feedback.

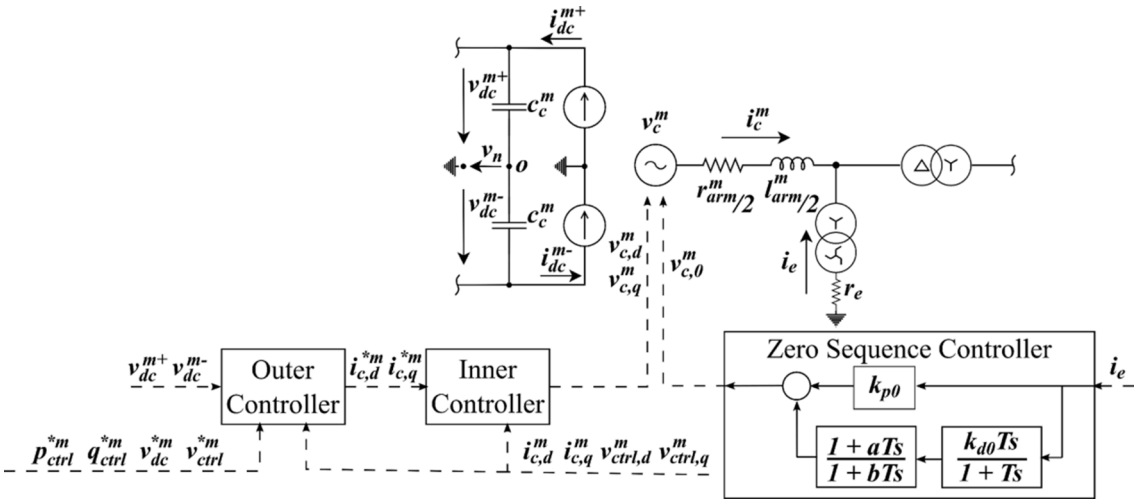

Fig. 15. Controller to enhance system stability during asymmetrical operation.

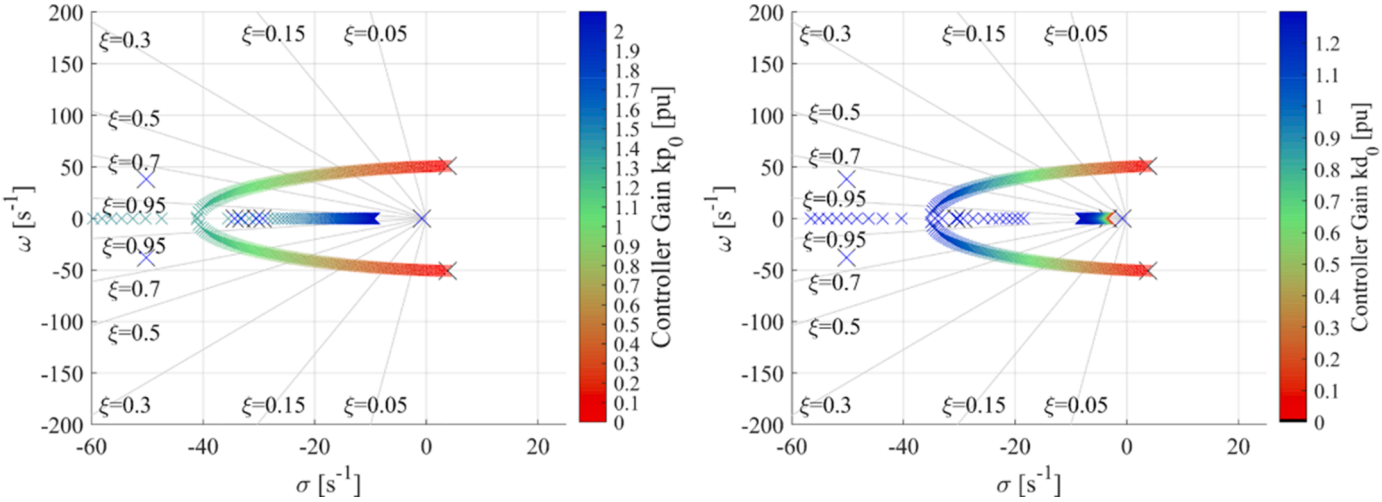

Fig. 16. Root locus of the system for different values of k_{p0} (left) and k_{d0}(right).

4.2. Influence of the grounding system inductance

The grounding inductance is also decisive for the asymmetrical DC operation since it impacts the transient response of the system. From the small-signal stability perspective, its influence on the eigenvalues is proved in Fig. 10 for a constant grounding resistance (30.625 Ω - 0.1 p. u.). The initial conditions are those shown in Fig. 4.

There is a single mode affected by the grounding inductance. The damping and the frequency of the mode decrease as inductance increases, leading to system instability if the grounding inductance reaches large enough values (around 9 p.u. – 3067 H), which are typical if a star point reactor is used as a grounding method.

Fig. 11 indicates that this mode is the same as in the case of the grounding resistance since the same states participate in the mode. Observe that the grounding inductance does not affect the participation of DC voltages. However, its increment rises the participation of earth current and reduces the participation of DC currents.

The observability of the mode against the inductance value of the grounding system is presented in Fig. 12 (left). The mode is observable in DC voltages and currents as well as in earth current, but as inductance rises the observability increases in DC voltages while decreases in earth current and DC currents. Regarding the AC system, as the mode is only observable in the zero-sequence variables for any value of grounding impedance, it does not spread beyond the delta-winding of the transformer and, thus, it does not affect the stability of the remaining AC system.

Fig. 12 (right) indicates that the main inputs that can control the mode continue to be the zero-sequence voltage reference of the monopolar station ($v^{*m}_{c,0}$) and the active power references of the bipolar station (p^{*b+}_{ctrl} and p^{*b-}_{ctrl}), regardless of the inductance.

4.3. Influence of the initial DC current before the disturbance

This section delves into the impact that the DC current has on the small-signal stability, specifically, in the mode related to DC asymmetrical operation. For this analysis the grounding resistance and inductance considered are 0 p.u. and 1.63 p.u., respectively.

To perform the DC current sweep, the active power references of the bipolar HVDC station are changed from those of the load flow shown in Fig. 4, so that the complete DC current range is evaluated. The movement of the eigenvalues against the initial DC current is displayed in Fig. 13.

Fig. 13 shows that there are several modes affected by DC current, but the least damped and potentially unstable is the one related to DC asymmetrical operation. Indeed, it is worth noting that DC current directly affects the damping of this mode, whilst hardly modifying its frequency. Furthermore, the mode is stable for a negative DC current

direction, even considering a zero value of grounding resistance. Thus, this fact confirms that the direction of the DC current determines the system's stability.

For the sake of simplicity, the participation factors, observability, and mode controllability are not shown since they remain unchanged for any value of the DC current, maintaining the values shown in Fig. 8 and Fig. 9 for a zero-grounding resistance.

4.4. Influence of other system parameters

Fig. 14 shows the sensitivity of the mode related to the DC asymmetrical operation, where the sensitivity of the mode λ to the element a_{kj} of the state matrix A is defined as $s = \frac{d\lambda}{da_{kj}} = \frac{d\sigma}{da_{kj}} + j\frac{d\omega}{da_{kj}}$.

Observe that the main parameters affecting the mode are the zero-sequence impedance ratio, the DC voltage and DC current, the line impedance ratio, and the equivalent capacitance of the bipolar HVDC station.

The zero-sequence resistance $\left(r_0 = \frac{r^m_{arm}}{2} + 3r_e\right)$ to inductance $\left(l_0 = \frac{l^m_{arm}}{2} + l_e\right)$ ratio represents the highest impact on the real part of the mode and an important weight in its frequency. Both the real and imaginary parts of the mode diminish as this ratio rises. The resistance to inductance ratio of the DC line has the same trend but its weight is much smaller.

The parameter composed of the initial DC current and DC voltage of the bipolar station, together with its equivalent capacitance (c^b), also modifies the real and imaginary parts of the mode. Observe that this element represents an equivalent conductance to capacitance ratio. Thus, when the DC current is positive, this equivalent conductance is negative and reduces the damping of the system.

There is another element of the state matrix that depends on the zero-sequence inductance and together with the equivalent capacitance of the bipolar HVDC station represent the main elements that affect the frequency of the mode.

Since the mode shows no noticeable sensitivity to the parameters of the controllers, it cannot be controlled by the typical control loops shown in Fig. 3.

5. Zero-sequence controller design

The results obtained suggest that it is possible to design a controller aimed at damping the mode related to DC asymmetric operation. Given the impact of the grounding impedance on the mode, the controller will be implemented in the monopolar station.

From a protection design perspective, a low grounding resistance allows for easy fault detection and faster tripping of relays, but it can lead to the development of an unstable or poorly damped mode. Therefore, the proposed controller is designed to improve the stability for low grounding resistance scenarios, regulating the zero-sequence voltage according to the earth current measurement. The controller is shown in Fig. 15 and has two main control actions, provided by the upper and the lower path, which may or may not be combined.

In the upper path, the gain k_{p0} acts as a virtual grounding resistance so that it can be used to enhance the stability for any resistance value. Therefore, the movement of the mode as a function of this gain is similar to the movement presented in Fig. 7 for a grounding resistance sweep, as displayed in the left graph in Fig. 16. For that reason, the steady-state operating point after the disturbance is changed depending on its value.

The lower path of the controller in Fig. 15 has the advantage of working only during the transient, without affecting the steady state. The right graph in Fig. 16 displays the change of the mode with the rise of k_{d0} for a zero-grounding resistance when $k_{p0} = 0$. The damping of the unstable mode greatly enhances, even becoming an overdamped mode. Since the controller only acts during the transient and does not modify the effective grounding resistance in case of faults, it hardly affects the performance of protections.

The tuning of the proposed controller must be done considering the grounding impedance and the entire operating range of the HVDC system to achieve an appropriate response under all circumstances.

6. Conclusions

This paper presented a new small-signal stability model for the analysis of the asymmetrical DC operation in HVDC systems with different HVDC station topologies and without galvanic isolation between them. The small-signal model includes the grounding system and equations for each pole separately; these considerations differentiate it from existing models and constitute a novelty. The new model has been validated against EMT simulations.

The advantages of this model are: (1) it allows to identify stability issues related to the asymmetrical DC operation that cannot be detected with other small-signal models, and (2) it can be applied to larger HVDC systems. Although time-domain simulations can represent this type of instability, they are not an efficient tool to perform stability studies on large systems, nor do they provide an easy method to recognize the main parameters and variables that are involved in a specific oscillation of the system. In addition, the present study has confirmed that the small-signal analysis provides an additional requirement in terms of stability of the whole system that should be considered in the design of the grounding system of an HVDC network. The small-signal model may also be used to develop controllers that improve the dynamic response of the system during asymmetrical DC operation, tune them, or select their best location in the case of larger HVDC systems.

Future works should explore the implications of the asymmetrical DC operation in systems with other control strategies and in larger DC grids.

Funding

Grant PID2019-104449RB-I00 funded by MCIN/AEI/10.13039/501100011033.

CRediT authorship contribution statement

Jesús Serrano-Sillero: Conceptualization, Methodology, Software, Validation, Writing – original draft, Writing – review & editing. **M. Ángeles Moreno:** Conceptualization, Methodology, Supervision, Writing – review & editing.

Declaration of Competing Interest

The authors declare no conflict of interest. The funders had no role in the design of the study; in the collection, analyses, or interpretation of data; in the writing of the manuscript, or in the decision to publish the results.

Data availability

No data was used for the research described in the article.

Acknowledgments

Funding for APC: Universidad Carlos III de Madrid (Read & Publish Agreement CRUE-CSIC 2022).

Appendix

Tables 1 and 2

Table 1
System parameters.

Description	Symbol	Value	Base values		
			Voltage V_b	Power S_b	Frequency ω_b
Grid frequency	ω_g	1 p.u.	–	–	100π rad/s
Equivalent impedance of AC networks	l_g	0.0265 p.u.	380 kV	800 MVA	
	r_g	0.0027 p.u.			
Equivalent impedance of transformers	l^m_{trf}	0.18 p.u.	380/200 kV		
	r^m_{trf}	0.006 p.u.			
	l^b_{trf}	0.36 p.u.			
	r^b_{trf}	0.012 p.u.			
Arm impedance of converters	l^m_{arm}	0.1815 p.u.	200 kV		
	r^m_{arm}	0.0605 p.u.			
	l^b_{arm}	0.363 p.u.			
	r^b_{arm}	0.121 p.u.			
Equivalent capacitance of converter submodules (c^b_c also includes the capacitance of the DC line)	c^m_c	28.8634 p.u.	± 350 kV	400 MVA	
	c^b_c	28.9817 p.u.			
Equivalent parameters of the DC line	c_{line}	0.1183 p.u.			
	r_{line}	0.0072 p.u.			
	l_{line}	0.1920 p.u.			
Resistance between the neutral point of the zig-zag transformer and ground (changed along the paper)	r_e	0 p.u.			
Equivalent default inductance of the zig-zag transformer (changed along the paper)	l_e	1.6327 p.u.			

Table 2
Control parameters.

Description	Outer controller								Inner controller			
Symbol	kp_{vdc}	ki_{vdc}	kp_p	ki_p	kp_{vac}	ki_{vac}	kp_q	ki_q	kp_i	ki_i	l^m_{cc}	l^b_{cc}
Value	7.465	253.81	0	33	0	30	0	30	0.48	149	0.27075	0.1815

References

[1] European network of transmission system operators for electricity (ENTSO-E), "HVDC links in system operations," Tech. Paper, Dec. 2019. [Online] Available: https://eepublicdownloads.entsoe.eu/clean-documents/SOC%20documents/20191203_HVDC%20links%20in%20system%20operations.pdf.

[2] A. Alassi, S. Bañales, O. Ellabban, G. Adam, C. MacIver, HVDC transmission: technology review, market trends and future outlook, Renew. Sustain. Energy Rev. 112 (2019) 530–554. Sep.

[3] W. Leterme, P. Tielens, S. De Boeck, D. Van Hertem, Overview of grounding and configuration options for meshed HVDC grids, IEEE Trans. Power Del. 29 (6) (2014) 2467–2475. Dec.

[4] G.P. Adam, I.A. Gowaid, S.J. Finney, D. Holliday, B.W. Williams, Review of DC–DC converters for multi-terminal HVDC transmission networks, IET Power Electron 9 (2) (2016) 281–296. Feb.

[5] D. Jovcic, M. Taherbaneh, J.P. Taisne, S. Nguefeu, Developing regional, radial DC grids and their interconnection into large DC grids, in: Proc. IEEE PES General Meeting, 2014, pp. 1–5, https://doi.org/10.1109/PESGM.2014.6939425.

[6] J.D. Paez, D. Frey, J. Maneiro, S. Bacha, P. Dworakowski, Overview of DC-DC converters dedicated to HVdc grids, IEEE Trans. Power Del. 34 (1) (2019) 119–128. Feb.

[7] E. Berne, G. Bergna, P. Egrot, Q. Wolff, Earth currents in HVDC grids: an example based on 5 terminal bipolar configurations, in: 16th Eur. Conf. Power Electron. and Appl., 2014, pp. 1–10, https://doi.org/10.1109/EPE.2014.6910729.

[8] M.J. Pérez-Molina, D.M. Larruskain, P.Eguía López, G. Buigues, Challenges for protection of future HVDC grids, Front. Energy Res. 8 (2020). Feb., Art. no. 33.

[9] M. Muniappan, A comprehensive review of DC fault protection methods in HVDC transmission systems, Prot. Control Mod. Power Syst. 6 (1) (2021) 1–20. Jan.

[10] F. Gonzalez-Longatt, J.L. Rueda, M.A.M.M. van der Meijden, Effects of grounding configurations on post-contingency performance of MTDC system: a 3-Terminal example, in: 50th Int. Univ. Power Eng. Conf. (UPEC), 2015, pp. 1–6, https://doi.org/10.1109/UPEC.2015.7339912.

[11] A. Junyent-Ferre, P. Clemow, M.M.C. Merlin, T.C. Green, Operation of HVDC modular multilevel converters under DC pole imbalances, in: 16th Eur. Conf. Power Electron. and Appl., 2014, pp. 1–10, https://doi.org/10.1109/EPE.2014.6911011.

[12] M. Wang, W. Leterme, G. Chaffey, J. Beerten, D. Van Hertem, Pole rebalancing methods for pole-to-ground faults in symmetrical monopolar HVDC grids, IEEE Trans. Power Del. 34 (1) (2019) 188–197. Feb.

[13] M. Wang, J. Beerten, D. Van Hertem, Pole voltage balancing in HVDC systems: analysis and technology options, in: Proc. 2019 IEEE Milan PowerTech, 2019, pp. 1–6, https://doi.org/10.1109/PTC.2019.8810816.

[14] Y. Tao, B. Li, T. Liu, Pole-to-ground fault current estimation in symmetrical monopole high-voltage direct current grid considering modular multilevel converter control, Electron. Lett. 56 (8) (2020) 392–395. Apr.

[15] S.D. Tavakoli, E. Prieto-Araujo, E. Sánchez-Sánchez, O. Gomis-Bellmunt, Interaction assessment and stability analysis of the MMC-Based VSC-HVDC link, Energies 13 (8) (2020). Apr., Art. no. 2075.

[16] B. Qin, W. Liu, R. Zhang, T. Ding, J. Liu, Small-signal stability analysis and optimal control parameters design of MMC-based MTDC transmission systems, IET Gener. Transm. Dis. 14 (21) (2020) 4675–4683. Nov.

[17] B. Rehman, C. Liu, W. Wei, C. Fu, H. Li, Applications of eigenvalues in installation of multi-infeed HVDC system for voltage stability, Int. Trans. Elect. Energy Syst. 30 (12) (2020). Dec., Art. no. e12645.

[18] M. Amin, M. Molinas, J. Lyu, X. Cai, Impact of power flow direction on the stability of VSC-HVDC seen from the impedance nyquist plot, IEEE Trans. Power Electron. 32 (10) (2017) 8204–8217. Oct.

[19] Q. Fu, W. Du, H. Wang, B. Ren, X. Xiao, Small-signal stability analysis of a VSC-MTDC system for investigating DC voltage oscillation, IEEE Trans. Power Syst. 36 (6) (2021) 5081–5091. Nov.

[20] Q. Fu, W. Du, H.F. Wang, B. Ren, Analysis of small-signal power oscillations in MTDC power transmission system, IEEE Trans. Power Syst. 36 (4) (2021) 3248–3259. Jul.

[21] J. Zhu, et al., Coherence analysis of system characteristics and control parameters for Hybrid HVDC transmission systems based on small-signal modeling, IEEE J. Emerg. Sel. Top. Power Electron. 9 (6) (2021) 7436–7446. Dec.

[22] C. Guo, A. Zheng, Z. Yin, C. Zhao, Small-signal stability of hybrid multi-terminal HVDC system, Int. J. Elect. Power Energy Syst. 109 (2019) 434–443. Jul.

[23] J. Serrano-Sillero, M.Á. Moreno, A. Morales, HVDC grids with heterogeneous configuration stations under DC asymmetrical operation, Int. J. Elect. Power Energy Syst. 113 (2019) 449–460. Dec.

[24] CIGRE WG, "Guide for the development of models for HVDC converters in a HVDC grid," CIGRE Brochure, Paris, France, Tech. Rep. TB 604 2013 B4-57, 2014.

[25] T. Abedin, et al., Dynamic modeling of HVDC for power system stability assessment: a review, issues, and recommendations, Energies 14 (16) (2021). Aug., Art. no. 4829.

[26] A.B. Iskakov, I.B. Yadykin, Lyapunov modal analysis and participation factors applied to small-signal stability of power systems, Automatica 132 (2021). Oct., Art. no. 109814.